

# Suppression of spin-pumping by a MgO tunnel-barrier

O. Mosendz,<sup>1,\*</sup> J. E. Pearson,<sup>1</sup> F. Y. Fradin,<sup>1</sup> S. D. Bader,<sup>1,2</sup> and A. Hoffmann<sup>1,2</sup>

<sup>1</sup>Materials Science Division, Argonne National Laboratory, Argonne, IL 60439, USA

<sup>2</sup>Center for Nanoscale Materials, Argonne National Laboratory, Argonne, IL 60439, USA  
(Dated: May 23, 2022)

Spin-pumping generates pure spin currents in normal metals at the ferromagnet (F)/normal metal (N) interface. The efficiency of spin-pumping is given by the spin mixing conductance, which depends on N and the F/N interface. We directly study the spin-pumping through an MgO tunnel-barrier using the inverse spin Hall effect, which couples spin and charge currents and provides a direct electrical detection of spin currents in the normal metal. We find that spin-pumping is suppressed by the tunnel-barrier, which is contrary to recent studies that suggest that the spin mixing conductance can be enhanced by a tunnel-barrier inserted at the interface.

PACS numbers: 72.25.Rb, 75.47.-m, 76.50.+g

Developments in spintronics provide new insights in the physics of spin related phenomena. One new research direction is to explore pure spin currents, which are independent of charge currents [1, 2]. Pure spin currents can be generated via a spin-polarized charge current injection from ferromagnets [3, 4], spin Hall effects [5, 6], or spin-pumping [7, 8]. The last differs from the other two mechanisms, since it uses magnetization dynamics rather than electric charge currents for the pure spin current generation. The spin current in this case is generated by a precessing magnetization in the ferromagnetic layer at the ferromagnet (F)/normal metal (N) interface. The precessing magnetization at the F/N interface acts as a peristaltic spin-pump, which creates a dynamic spin accumulation in the normal metal diffusing away from the interface. Non-local effects in the magnetization dynamics due to spin-pumping were studied extensively [9, 10, 11, 12] and revealed a new coupling mechanism between ferromagnets separated by a non-magnetic material. Furthermore, studies, which used spin-pumping as a spin current generator enabled quantification of spin Hall effects in normal metals [13, 14]. For practical applications it would be useful to increase the efficiency of spin-pumping. To this end, recent work by Moriyama *et al.* [15] suggests that spin-pumping may be significantly enhanced by an insulating (I) tunnel-barrier inserted at the interface between a ferromagnet and normal metal. This result contrasts with theoretical predictions [16], which suggests that sizable spin-pumping requires a transparent interface between the ferromagnet and normal metal.

To resolve this problem a detection scheme sensitive to the pure spin currents in the normal metal is needed. Inverse spin Hall effect (ISHE) measurements [13, 14] are a good approach to detect any enhancement of spin pumping across the F/I/N structure, since they are directly sensitive to pure spin currents and unaffected by other spurious voltages across the tunnel-barrier. The *dc* part

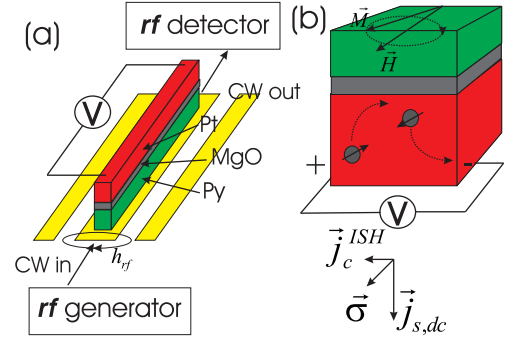


FIG. 1: (Color online) Experimental setup. (a) Schematic of the Py/MgO/Pt structure integrated into the coplanar waveguide. (b) ISHE detection schematic. The precessing magnetization in the ferromagnet generates a spin current in the adjacent normal metal. This spin current leads to a charge current in the normal metal due to a preferential scattering direction for electrons carrying the pumped spin accumulation. The charge current is orthogonal to the spin current direction and the spin polarization. A voltage difference due to the ISHE is measured between the ends of Pt/MgO/Py strip. Note that orientation in (a) and (b) is changed for illustrative purposes.

of the spin current in the normal metal generated by the spin-pumping, gives rise to a transverse charge current  $\vec{j}_c^{ISH} = \gamma(2e/\hbar)[\vec{j}_{s,dc} \times \vec{\sigma}]$  via the ISHE [see Fig. 1(b)] where  $\gamma$  is the materials-specific spin Hall angle,  $\vec{j}_{s,dc}$  is the spin current and  $\vec{\sigma}$  is the spin polarization. Any enhancement of spin-pumping will manifest itself as an increased voltage due to the ISHE. Thus comparing  $\vec{j}_c^{ISH}$  for two structures: (i) F/N and (ii) F/I/N enables us to investigate the spin-pumping strength in the case of an insulating tunnel-barrier compared to a transparent interface. As we show in this Letter, spin-pumping is actually suppressed by the tunneling barrier.

We integrated different F/N heterostructures into coplanar waveguides with additional leads for *dc* voltage measurements along the sample. A schematic is shown in Fig. 1(a) for a  $15\text{Ni}_{80}\text{Fe}_{20}$  (Py)/3MgO/15Pt

\*Electronic address: mosendz@anl.gov

heterostructure, where integers indicate the thicknesses of the individual layers in nm, with lateral dimensions of  $2.92 \text{ mm} \times 20 \text{ }\mu\text{m}$ . The heterostructure was prepared by optical lithography, sputter deposition, and lift-off on a GaAs substrate. Subsequently we prepared Ag electrodes in contact with the Pt-layer for the voltage measurements, covered the whole structure with 100-nm thick MgO (for *dc* insulation between the heterostructure and waveguide), and defined on top a 30- $\mu\text{m}$  wide and 200-nm thick Au coplanar waveguide. Two control samples were prepared: a 15 nm Py/15 nm Pt sample without the 3 nm MgO tunnel-barrier and a 15Py sample without the normal metal.

The ferromagnetic resonance (FMR) was excited at 4-GHz *rf* with 100-mW power, while applying a *dc* magnetic field  $\vec{H}_{dc}$  at  $\alpha = 45^\circ$  with respect to the waveguide. The FMR signal was determined from the impedance of the waveguide [12]; simultaneously the *dc* voltage was measured as a function of  $\vec{H}_{dc}$ . This is shown in Fig. 2 for Py/Pt, Py/MgO/Pt and Py. The FMR peak positions for all samples are similar and are described by the Kittel formula with a saturation magnetization for  $\text{Py}M_s = 851 \text{ G}$  (see Fig. 2). The FMR linewidths (half width at half maximum) extracted from fitting to Lorentzian absorption functions are  $\Delta H_{\text{Pt}/\text{Py}} = 16.9 \text{ Oe}$  for Py/Pt,  $\Delta H_{\text{Pt}/\text{MgO}/\text{Py}} = 12.3 \text{ Oe}$  for Py/MgO/Pt, and  $\Delta H_{\text{Py}} = 12.7 \text{ Oe}$  for Py. The difference in FMR linewidths for the Pt/Py and Py samples can be attributed to the loss of spin momentum in Pt [17]. The linewidth for the Py/MgO/Pt sample is close to  $\Delta H_{\text{Py}}$ , which already suggests that spin-pumping is suppressed by the tunnel-barrier, and non-local damping does not influence the Py layer in the Py/MgO/Pt structure.

The *dc* voltage measured along the samples is shown with solid symbols in Fig. 2. We observe a resonant increase of the *dc* voltage along the sample at the FMR position. The signal measured for Pt/Py has two contributions: (i) anisotropic magnetoresistance (AMR) and (ii) ISHE [13]. The voltage due to AMR is:

$$V_{AMR} = I_{rf} \Delta R_{AMR} \frac{\sin(2\theta)}{2} \frac{\sin(2\alpha)}{2} \cos \varphi_0, \quad (1)$$

where  $I_{rf}$  is the *rf* current, which flows through Py,  $\Delta R_{AMR}$  is the AMR in Py,  $\varphi_0$  is the phase angle between magnetization precession and driving *rf* field, and  $\theta$  is the cone angle of precession. The voltage due to ISHE is:

$$V_{ISH} = -\frac{\gamma g_{\uparrow\downarrow} e L \lambda_{sd} \omega}{2\pi \sigma_{Pt} t_{Pt}} \sin \alpha \sin^2 \theta \tanh \left( \frac{t_{Pt}}{2\lambda_{sd}} \right), \quad (2)$$

where  $g_{\uparrow\downarrow}$  is the spin mixing conductance,  $e$  is the electron charge,  $L$  is sample length,  $\lambda_{sd}$  is the spin diffusion length in Pt,  $\omega$  is the FMR frequency,  $\sigma_{Pt}$  is Pt conductivity, and  $t_{Pt}$  is the thickness of the Pt layer.

As shown in Fig. 2(a), we used Eq. (1) for the AMR contribution (dashed line) and Eq. (2) for the ISHE contribution (dotted line) to fit the voltage measured for the

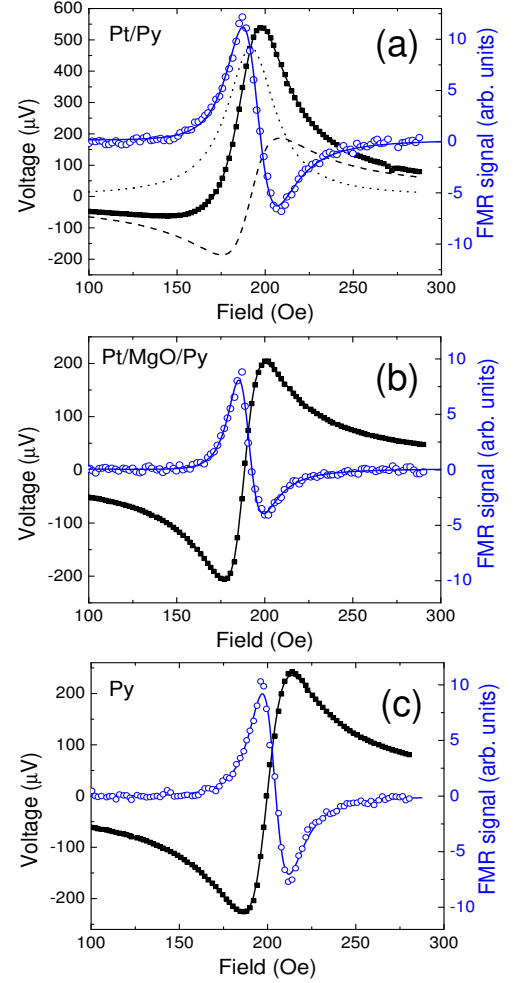


FIG. 2: (Color online) FMR derivative spectra are shown (blue open symbols) for (a) Py/Pt, (b) Py/MgO/Pt, and (c) Py samples. Solid lines are fits to a Lorentzian FMR absorption function. The voltage measured along the samples *vs.* field  $H_{dc}$  is shown with black solid symbols. Black dotted and dashed lines are fits to Eqs. (1) and (2), respectively in (a). The solid line in (a) shows the combined fit for the Py/Pt sample. Solid lines in (b) and (c) represent fits of the measured voltage to Eq. (1) only.

Py/Pt sample. By using a literature value of  $\lambda_{sd} = 10 \text{ nm}$  for Pt [18], the only remaining adjustable parameters are the *rf* driving field  $h_{rf} = 4.2 \text{ Oe}$  and the spin Hall angle for Pt  $\gamma = 0.0115 \pm 0.0003$  [13]. In contrast, the single layer Py sample, which is not affected by spin-pumping, shows a voltage signal, which is described only by the AMR part. A similar signal is observed for the Py/MgO/Pt sample, where the insulating tunnel-barrier is present. The relative strengths of the ISHE and AMR signals depends on the orientation of the applied field with respect to the waveguide. In Figs. 3(a) and (c) we show experimental data for several angles of the ap-

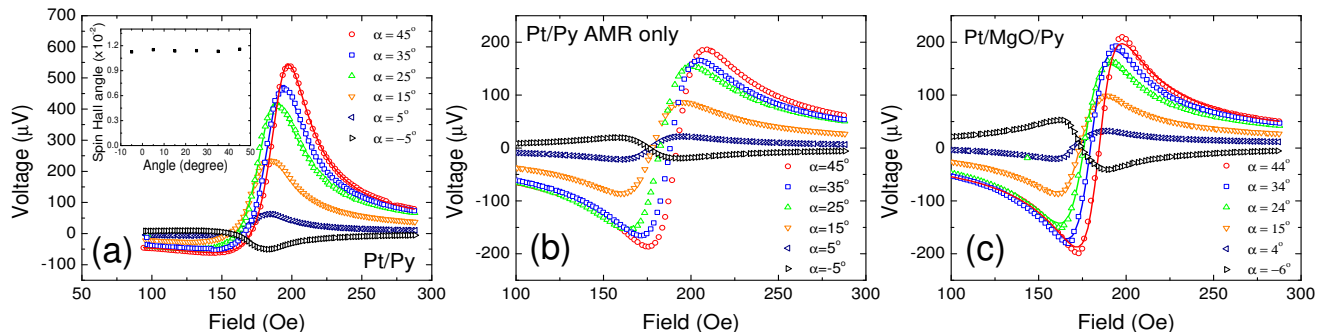


FIG. 3: (Color online) Dependence of the measured voltage on the angle  $\alpha$  of the applied field with respect to the waveguide axis. (a) Total measured voltage for the Pt/Py sample. The inset shows values of the spin Hall angle as a function of  $\alpha$ . (b) AMR contribution of the measured voltage for the Pt/Py sample and (c) total measured voltage for the Pt/MgO/Py sample. Note that signals in (b) and (c) are similar.

plied field for the Py/Pt and Py/MgO/Pt samples. The measured voltage is consistent with the theoretical prediction, and results in a constant value of the spin Hall angle in Pt, see inset in Fig. 3(a). AMR and ISHE contributions of the measured voltage can be separated, when the data is fitted to the theoretical model described by Eqs. (1) and (2). In Fig. 3(b) we plot the AMR contribution of the signal measured in the Py/Pt sample. The AMR contribution of the Py/Pt sample is the same as the total voltage measured along the Py/MgO/Pt sample, shown in Fig. 3(c), which indicates that there is no ISHE on the Py/MgO/Pt sample and consequently there is no spin current in the Pt layer. Our results show unambiguously that spin-pumping is suppressed when a 3-nm thick MgO tunnel-barrier is inserted at the Py/Pt interface.

In conclusion, we performed FMR with simultaneous transverse voltage measurements on Py/Pt and Py/MgO/Pt samples. We showed that in the case of Py/Pt, where spin-pumping is present, a transverse voltage has contributions from anisotropic magnetoresistance and inverse spin Hall effect. The transverse voltage for

the Py/MgO/Pt sample has only an anisotropic magnetoresistance contribution. FMR studies showed that non local damping does not affect the Py layer in the structure with a tunnel barrier in contrast with the transparent interface. This result confirms earlier theoretical predictions that a tunnel-barrier suppresses spin-pumping. The phenomenon, observed in Ref. 15 appears qualitatively similar to the predictions of the spin-pumping formalism, however the spin-pumping detection scheme utilized in the Moriyama's experiment may be sensitive to a non-equilibrium spin accumulation inside the ferromagnetic layer itself, caused potentially by structural imperfections. In this case the tunnel barrier will act as a non-intrusive probe of the spin-splitting of the chemical potentials in the ferromagnet induced by the magnetization dynamics [19]. To this end our studies show that tunnel barriers inserted at the F/M interface will not be useful for amplification of spin pumping.

We thank G. Mihaĵlović and G.E.W. Bauer for valuable discussions. This work was supported by the U.S. Department of Energy, Office of Science, Basic Energy Sciences under contract No. DE-AC02-06CH11357.

- 
- [1] C. Chappert and J.-V. Kim, *Nat. Phys.* **4**, 837 (2008).  
[2] A. Hoffmann, *Phys. Stat. Sol. (c)* **4**, 4236 (2007).  
[3] M. Johnson and R. H. Silsbee, *Phys. Rev. Lett.* **55**, 1790 (1985).  
[4] F. J. Jedema, A. T. Filip, and B. J. van Wees, *Nature* **410**, 345 (2001).  
[5] M. Dyakonov and V. Perel, *Phys. Lett. A* **35**, 459 (1971).  
[6] J. Hirsch, *Phys. Rev. Lett.* **83**, 1834 (1999).  
[7] B. Heinrich, Y. Tserkovnyak, G. Woltersdorf, A. Brataas, R. Urban, and G. E. W. Bauer, *PRL* **90**, 187601 (2003).  
[8] Y. Tserkovnyak, A. Brataas, and G. E. W. Bauer, *Phys. Rev. Lett.* **88**, 117601 (2002).  
[9] G. Woltersdorf, O. Mosendz, B. Heinrich, and C. H. Back, *Phys. Rev. Lett.* **99**, 246603 (2007).  
[10] O. Mosendz, G. Woltersdorf, B. Kardasz, B. Heinrich, and C. H. Back, *Phys. Rev. B* **79**, 224412 (2009).  
[11] B. Kardasz, O. Mosendz, B. Heinrich, Z. Liu, and M. Freeman, *J. Appl. Phys.* **103**, 07C509 (2008).  
[12] O. Mosendz, B. Kardasz, and B. Heinrich, *J. Appl. Phys.* **103**, 07B505 (2008).  
[13] O. Mosendz, J. E. Pearson, G. E. W. Bauer, S. D. Bader, and A. Hoffmann, *arXiv:0911.2725v1*.  
[14] E. Saitoh, M. Ueda, H. Miyajima, and G. Tatara, *Appl. Phys. Lett.* **88**, 182509 (2006).  
[15] T. Moriyama, R. Cao, X. Fan, G. Xuan, B. K. Nikolic, Y. Tserkovnyak, J. Kolodzey, and J. Q. Xiao, *Phys. Rev. Lett.* **100**, 067602 (2008).  
[16] A. Brataas, Y. Tserkovnyak, G. E. W. Bauer, and B. I. Halperin, *Phys. Rev. B* **66**, 060404 (2002).  
[17] R. Urban, G. Woltersdorf, and B. Heinrich, *Phys. Rev.*

- Lett. **87**, 217204 (2001).
- [18] H. Kurt, R. Loloee, K. Eid, J. W. P. Pratt, and J. Bass, Appl. Phys. Lett. **81**, 4787 (2002).
- [19] Y. Tserkovnyak, T. Moriyama, and J. Q. Xiao, Phys. Rev. B **78**, 020401 (2008).